Journal of Molecular Catalysis A: Chemical 325 (2010) 25–35

Contents lists available at ScienceDirect

Journal of Molecular Catalysis A: Chemical

journal homepage: www.elsevier.com/locate/molcata

Characterization of alumina-supported palladium oxide catalysts used in the oxidative coupling of 4-methylpyridine

Luke M. Neal, Samuel D. Jones, Michael L. Everett, Gar B. Hoflund, Helena E. Hagelin-Weaver*

Department of Chemical Engineering, University of Florida, Gainesville, FL 32611, United States

ARTICLE INFO

Article history:
Received 30 September 2009
Received in revised form 19 March 2010
Accepted 19 March 2010
Available online 30 March 2010

Keywords:
Pd/Al_2O_3
4-Methylpyridine
C–H activation
XPS
TEM

ABSTRACT

A number of palladium and palladium oxide on alumina catalysts for the oxidative coupling of 4-methylpyridine were characterized using X-ray photoelectron spectroscopy (XPS), transmission electron microscopy (TEM) and X-ray diffraction (XRD) to obtain more information about the properties that govern these reactions.

The most active catalysts, the impregnated and precipitated PdO/n-Al_2O_3(+), were found to have very broad Pd 3d peaks, suggesting the presence of both PdO_2 and Pd^0, in addition to PdO, on the surface. This could be due to strong metal–support interactions, which result in more electrophilic palladium or a reduced palladium catalyst that is easier to reoxidize, both of which are expected to result in high catalytic activities. As the PdO is completely reduced to Pd metal on spent catalysts (according to XPS and XRD), facilitated reoxidation could be important in this reaction. While reoxidation is a potential deactivation pathway, carbon deposition is also evident in the XPS spectra and this could block active sites. In contrast, both the XPS and the XRD data indicate that Pd leaching into the reaction solution is not a significant deactivation pathway in the PdO/n-Al_2O_3(+) catalyst system.

The nm-sized fine structure observed in the supports of the PdO/γ-Al_2O_3 and PdO/n-Al_2O_3(+), together with their measured activities compared to the poorly active PdO/n-Al_2O_3(−) catalyst with no such fine structure, supports our hypothesis that low-coordination sites on a support can result in strong metal–support interactions and very active catalysts. Highly active crystalline PdO particles with sizes of 5 nm or below may explain the observed lack of correlation between the measured Pd surface area (which should correlate with the PdO surface area) and the catalytic activity.

1. Introduction

Palladium is one of the more versatile active metals since it can serve as a catalyst in a large number of reactions [1–4]. Not only is palladium a very efficient hydrogenation catalyst [5], it is also an excellent catalyst for both selective oxidation (such as hexane to benzene [6] and alcohols to aldehydes or ketones [7]) and complete oxidation of for example CO [8,9], CH_4 [4,10,11] and volatile organic compounds (VOCs) [12–14]. One important reaction that has received relatively limited attention is the C–H activation and C–C coupling of aromatic systems over palladium catalysts. Of these, the palladium-catalyzed oxidative coupling of 4-methyl pyridine to 4,4′-dimethyl-2,2′-bipyridine is of particular interest (Scheme 1). The bipyridine product has the ability to coordinate to transition metal cations and form complexes with interesting photo- and electro-chemical properties [15–20]. Organometallic bipyridine complexes are also very efficient catalyst systems [21,22]. The 4,4′-dimethyl-2,2′-bipyridine is a particularly important bipyridine due to the facile oxidation of the methyl groups in the four position [15,23,24], which allows further reaction and attachment of catalyst complexes to a support [25]. Moreover, the oxidative coupling of 4-methylpyridine to 4,4′-dimethyl-2,2′-bipyridine over palladium catalysts is a simple, environmentally friendly, one-step process, where water and the terpyridine are the only byproducts. This is, thus, an important alternative to the route of using expensive halogenated precursors to form the bipyridine, particularly since the latter is formed with an undesired halide byproduct. However, the coupling reaction is slow with relatively low yields [26], so significant improvements would be desirable.

The most commonly used palladium catalyst reported in the literature for this reaction is palladium on carbon (Pd/C), while commercial palladium on alumina (Pd/Al_2O_3) catalysts had been shown to be practically inactive [27–30]. In contrast, recent research studies have demonstrated that 5% palladium precipitated onto alumina nanoparticles (PdO/n-Al_2O_3) [31] or porous titania (PdO/p-TiO_2) [32] results in the highest yields reported to date for

* Corresponding author at: Department of Chemical Engineering, University of Florida, P.O. Box 116005, Gainesville, FL 32611, United States. Tel.: +1 352 392 6585; fax: +1 352 392 9513.
E-mail address: hweaver@che.ufl.edu (H.E. Hagelin-Weaver).

1381-1169/$ – see front matter © 2010 Elsevier B.V. All rights reserved.
doi:10.1016/j.molcata.2010.03.024

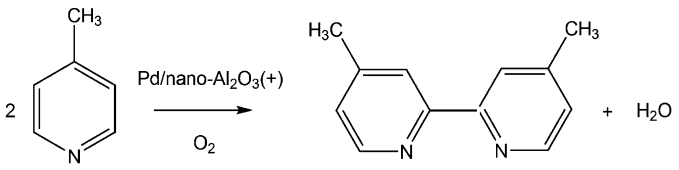

Scheme 1.

this palladium-catalyzed reaction, i.e. 2.5 g of product per g of catalyst or ~50 g/g palladium [33,34]. Previous results indicated that the catalytic activity was dependent on the alumina support and the preparation method used [33]. To this point, no systematic correlation between palladium dispersion and catalytic activity has been found.

As, no distinct correlation between catalyst properties and catalytic activity was previously determined, a more thorough catalyst characterization study is needed to further improve these catalysts. The catalysts have therefore been subjected to the following catalyst characterization techniques: (I) X-ray photoelectron spectroscopy (XPS) to probe the surface composition and chemical states of the Pd phase in the fresh and spent catalysts, (II) transmission electron microscopy (TEM) with energy dispersive spectroscopy (EDS) to image the structure and dispersion of prepared catalysts, as well as (III) X-ray diffraction (XRD) to determine the crystal structure of the catalyst supports and if the palladium on the surface can be detected with XRD. The objectives of this work were to characterize the Pd/PdO crystallites in fresh and selected reduced or spent catalysts for (1) crystallite size and dispersion, (2) oxidation state and electronic binding energy, and (3) support structure to determine if any of these properties correlate with the catalytic activity of the catalysts.

2. Experimental

2.1. Catalyst preparation and reaction

The commercial catalysts, 5% Pd/C (dry, reduced) and 5% Pd/Al_2O_3 were obtained from Alfa Aesar and used after drying at 105 °C for at least 1 h. A number of alumina-supported catalysts with 5% palladium loading were prepared using precipitation with sodium hydroxide and a calcination temperature of 350 °C as described in previous work [33] and were subjected to careful characterization. Unless otherwise stated, the prepared catalysts were used without reductive pretreatment. Therefore, they are most appropriately labeled as PdO on the support, i.e. PdO/n-Al_2O_3(+) [31], PdO/n-Al_2O_3(−) [35] and PdO/γ-Al_2O_3 [36].

The reactions were carried out by placing fresh calcined catalyst and doubly distilled 4-methylpyridine under reflux for 72 h [33]. After a complete reaction the catalyst was recovered using a glass micro-fiber filter and washed with chloroform to dissolve the product. The recovered spent catalyst was stirred in additional chloroform and filtered, followed by brief drying at room temperature before it was analyzed using XPS or XRD.

Reduced catalysts were prepared by reduction in 5% hydrogen in nitrogen for 1 h at 170 °C, outgassed in nitrogen at the same temperature for an additional hour, and then cooled to room temperature under continued nitrogen flow. As the catalysts are used in the reaction without reduction, i.e. in PdO form rather than as Pd metal, the reduction conditions are kept at low temperatures to reduce sintering of the palladium. The reduced catalyst samples were kept sealed in nitrogen until immediately before XPS and XRD sample preparation. One reduced PdO/n-Al_2O_3(+) catalyst was transferred to the reaction flask for reaction. While the brief room-temperature air exposure may result in some surface oxidation, it is not expected to cause significant oxidation of the Pd on the surface.

2.2. Chemisorption experiments

The chemisorption measurements were performed on *in situ* reduced catalysts, as described above. While PdO is necessary for the reaction, these measurements are done to obtain a qualitative measure on how the PdO is distributed on the surface (as it is expected that the measured Pd metal surface area correlates with the PdO distribution). A spent PdO/n-Al_2O_3(+) catalyst was outgassed in nitrogen at 170 °C for 1 h and then subjected to the same reductive pretreatment applied to the fresh catalysts before the CO adsorption experiments. The pulsed CO chemisorption technique was used to measure the amount of CO adsorbed on each catalyst, and the Pd surface area was calculated from these experiments assuming a 1:1 Pd:CO ratio. Even though there are likely bridged CO molecules (and perhaps some CO bound at hollow sites) present on the surface after adsorption, particularly on the low dispersion catalysts, a conservative 1:1 ratio was used to give a lower bound for the surface areas. Estimates of the Pd particle sizes were also made from these CO adsorption measurements for comparison with the TEM and XRD data. The details of the calculations for Pd dispersion, surface area and crystallite size are given in previous work [34].

2.3. X-ray photoelectron spectroscopy (XPS)

The fresh, spent or reduced catalyst powders were pressed into aluminum cups prior to insertion into the ultra-high vacuum (UHV) chamber (base pressure 1×10^{-10} Torr). XPS was performed using a double pass cylindrical mirror analyzer (PHI model 25-270 AR). Spectra were taken in retarding mode with a pass energy of 50 eV for surveys and 25 eV for high resolution spectra using a Mg Kα X-ray source (PHI 04-151). Data were collected and then digitally smoothed using a computer interface. A value for the C1s binding energy of 284.6 eV was assigned to correct for static charging [37].

The XPS spectra are presented in the figures without background subtraction. However, peak area analyses were carried out on spectra corrected using a linear background subtraction. The integrated peak areas were corrected for the atomic sensitivity factors [37] before the surface concentrations and elemental ratios were calculated. Due to the possible errors introduced while calculating background-subtracted peak areas and the uncertainties in the atomic sensitivity factors used, together with the fact that the catalyst compositions on these catalysts vary significantly in the near surface region, both laterally and vertically, only the trends in relative concentrations and the elemental ratios between catalysts are discussed.

Peak fittings using Gaussian functions for the peak shapes were also performed on the Pd $3d_{5/2}$ peaks after background subtraction to facilitate comparisons between catalysts. As each Gaussian function contains three parameters, the peak position, the peak width and the peak area, peak fitting is rather arbitrary if the exact peak positions and peak widths are not known, which is the case in this study. Therefore, the peak position and peak width of a reference PdO sample were used as the starting point in the peak fittings. Peaks of Pd^0 and "PdO_x" ($x > 1$) were then added at 334.9 and 337.5 eV with similar peak widths. Peak fitting was initiated by relaxing the peak position and the peak width slightly using an automatic fitting routine. The parameters of the Gaussian functions were then adjusted slightly manually to get the best fit. As there are nine parameters total to fit the Pd $3d_{5/2}$ peak, the actual values of the parameters are rather arbitrary. Therefore, the peak fitting is used mainly to aid in determining differences between the Pd $3d_{5/2}$ peaks from the various catalysts. The peak areas are only calculated to determine trends between catalysts and are not to be taken as absolute numbers. The best fits for the Pd $3d_{5/2}$ peaks are obtained by including the three states, PdO_x, PdO and Pd^0, for all catalysts.

2.4. Transmission electron microscopy (TEM)

TEM grids were prepared by dispersing the fresh calcined catalysts into water by ultrasonication and then placing a drop of the catalyst dispersion onto lacy carbon grids. After evaporation of the water, micrographs and EDS spectra were collected on a JEOL TEM 2010F, with a 200-kV electron source. Several TEM images were recorded at various locations on the sample and at different magnifications to confirm that the structures observed were present throughout the catalyst. For each catalyst representative images are presented in the figures.

2.5. X-ray diffraction (XRD)

The XRD data were gathered on a Philips powder X-ray diffractometer using Bragg–Brentano geometry with Cu-Kα radiation (λ = 1.54 Å). Diffraction patterns were obtained for selected calcined, reduced and spent catalysts. The catalyst powders were secured onto a glass slide with double-sided sticky tape. Average particle sizes were calculated from the line-broadening of the XRD peaks using the Scherrer equation (1).

$$d = \frac{K\lambda}{\mathrm{FWHM}\ \cos(\theta)} \quad (1)$$

In this equation K is a constant generally taken as unity, λ is the wavelength of the incident radiation, FWHM is the full width at half maximum and θ is the peak position. As the PdO and alumina-related peaks overlap in the XRD patterns, Philips ProFit software (v. 1.0, 1996) was used to deconvolute the overlapping peaks and determine the FWHM for each peak.

3. Results and discussion

While these reactions in very early research were carried out on supported "palladium metal" catalysts, such as Pd/C and Pd/Al_2O_3 rather than PdO-based catalysts [27–29], more recent studies have revealed that PdO is likely the active phase [26,33,34]. Looking at a suggested reaction mechanism, it is evident how an oxidized Pd species would facilitate the reaction (Fig. 1).

3.1. Proposed reaction mechanism

In the proposed catalytic cycle for the palladium-catalyzed coupling of 4-methylpyridine, the first step is most likely coordination of the pyridine nitrogen to a palladium atom on the surface (Fig. 1). The C–H activation is probably facilitated by an oxygen atom in close proximity to the palladium on the surface. The result of the C–H activation is a hydroxyl group on the surface and a pyridine bonded to palladium via a carbon rather than the nitrogen. After two consecutive C–H insertions, a reductive elimination gives a coordinated bipyridine (not shown in Fig. 1) which later desorbs to give the product. Also, water is formed from the two surface hydroxyl groups and desorbs leaving an oxygen vacancy on the surface. To close the catalytic cycle the surface oxygen must be regenerated. This step is likely not trivial, given the nature of the reaction. Consequently, the C–H activation and the reoxidation of the reduced catalyst are two candidates for the rate determining step of this reaction. It is expected that the properties of the support influence the palladium dispersion and thus also the number of active sites. The properties of the support may also affect the rates of some steps, but is not likely to alter the overall mechanism.

Table 1
Results from surface area and chemisorption measurements on the alumina supports used in the current study.

Support	Surface area [m^2/g]	NH_3[a] [S cm^3/g]	CO_2[b] [S cm^3/g]
n-Al_2O_3(+)	695	9.0	0.75
n-Al_2O_3(−)	275	8.3	0.6
BM Y-Al_2O_3	260	1.6	1.75

[a] NH_3 uptake in standard cm^3/g.
[b] CO_2 uptake in standard cm^3/g.

3.2. Reaction data

The reaction data and surface area measurements for some of the catalysts characterized in this study have been reported previously [33]. A summary of the relevant results has been included in Tables 1 (supports) and 2 (catalysts), along with subsequent measurements. Table 1 reveals that the acidic and basic surface properties (i.e. NH_3 and CO_2 uptake) are similar on the n-Al_2O_3(+) and n-Al_2O_3(−) supports, while the product yields are very different (Table 2). This indicates that other catalyst properties, such as support and PdO structure, likely influence dispersion and catalytic activity for these catalysts.

It is evident from the results that this is a catalytic rather than stoichiometric reaction. If no reoxidation takes place, there is only sufficient PdO on the surface to yield less than 0.1 g of product per g of catalyst before complete reduction of PdO. The >2.5 g of product per g of catalyst reported for the most active catalysts is more than an order of magnitude higher than the stoichiometric yield.

Included in Table 2 are results showing that an impregnated PdO/n-Al_2O_3(+) catalyst can be quite active, when using different batches of support and palladium precursor from those used to prepare the poorly performing catalyst in previous work [33] (Table 2, entries 8 vs. 9 and 10). The yields from an impregnated catalyst are reasonably reproducible as long as the same batch of $Pd(NO_3)_2$ and n-Al_2O_3(+) support is used. The cause of the sensitivity to the batch of precursors used for the impregnated catalysts is not evident as no such sensitivity has been observed for the precipitated catalyst (as long as the $Pd(NO_3)_2$ precursor does not contain substantial amounts of PdO before catalyst preparation [33]). This may be attributed to trace amount of contamination in the $Pd(NO_3)_2$ precursor or alumina support (such as chloride ions), which would be left on the surface of the catalyst since the impregnation method does not include a rinsing step. Differences in the crystallinity and phase of the n-Al_2O_3(+) can also potentially influence the catalyst since it may alter the palladium–support interactions.

To determine the importance of PdO in these reactions, a PdO/n-Al_2O_3(+) catalyst was reduced using the same reduction treatment as before the CO adsorption measurements. The reduced PdO/n-Al_2O_3(+) catalyst does exhibit some activity, with a product yield

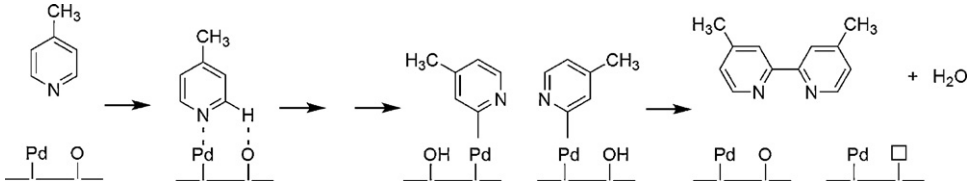

Fig. 1. Proposed reaction mechanism for the PdO-catalyzed oxidative coupling of 4-methylpyridine. (□) Marks an oxygen vacancy.

Table 2
Results from surface area, chemisorption and catalytic activity measurements.

Entry	Catalyst: 5% Pd loading[a]	Catalyst SA [m^2][b]	CO adsorbed [μmol/g cat]	Pd SA[c] [m^2/g]	Pd diameter [nm]	Yield [g/g cat][d]	Yield [g/g Pd]	TON[e]
1	Activated C[f,g]	695	110	5.2	4	1.8	36	90
2	Y-Al_2O_3 [f,g]	155	85	4.0	5	0.1	2.6	10
3	n-Al_2O_3(+)Pr[g]	180	205	9.7	2.1	2.8	56	75
4	n-Al_2O_3(+)Pr[g,h]	180	205	9.7	2.1	2.5	50	65
5	n-Al_2O_3(+)Pr[i,j]	ND	202	9.6	2.2	2.7	54	70
6	n-Al_2O_3(+)Pr Reduced[i]	ND	202	9.6	2.2	1.1	20	25
7	n-Al_2O_3(+)Pr Spent[i]	ND	52	2.5	8.4[k]	NA	NA	NA
8	n-Al_2O_3(+)Im[g]	170	70	3.3	6	0.2	4	15
9	n-Al_2O_3(+)Im[i]	ND	133	6.3	3.3	2.9	57	115
10	n-Al_2O_3(+)Im[h,i]	ND	133	6.3	3.3	2.6	51	105
11	n-Al_2O_3(−)[g]	155	15	0.7	30	0.3	5.8	105
12	BM y-Al_2O_3[g]	200	6.5	0.3	68	1.2	24	1000

[a] Commercial Pd/C and Pd/Al_2O_3 catalysts and bimodal (BM). γ-Al_2O_3 support from Alfa Aesar; n-Al_2O_3(+) and n-Al_2O_3(−) supports from NanoScale Inc.
[b] ND: not determined.
[c] The Pd surface area (SA) and average particle diameter have been calculated using 1:1 as the CO:Pd stoichiometry and a surface atom density of 1.27×10^{15} atoms/cm^2.
[d] NA: not applicable.
[e] TON: turnover number, i.e. number of moles of product formed per mole of surface Pd.
[f] Commercial catalyst.
[g] Results from previous work [33]. Only the average surface areas and particle sizes for the same batch of catalyst is reported.
[h] Repeated run on same batch of catalyst.
[i] Results from present work.
[j] Repeated run on different batch of catalyst.
[k] The low CO adsorption is consistent with carbon fouling according to XPS and XRD. Consequently, the calculated particle size is meaningless.

of 1.1 g/g of catalyst (Table 2). This yield is higher than for the commercial Pd/Al_2O_3, but significantly less than for the same unreduced catalyst. Consequently, reducing the PdO on the surface of the catalyst is detrimental to the reaction.

In addition, the CO chemisorption measurement on a spent catalyst after reductive treatment is included in Table 2. The result reveals that a lower amount of CO is adsorbed on the spent catalyst compared to the fresh catalysts after the same treatment. The calculated average particle size (~8.4 nm) is much larger than that calculated for reduced fresh catalyst (2 nm). The lower amount of CO adsorbed could be due to sintering of the palladium during the reductive treatment or during reaction, leaching of the palladium into the reaction solution, or carbon deposition that blocks the active palladium sites. The latter is suggested by XPS and XRD as discussed below.

3.3. XPS analysis

3.3.1. Survey spectra

The XPS survey spectrum obtained from the fresh, precipitated PdO/n-Al_2O_3(+) catalyst is displayed in Fig. 2. This spectrum is typical for these catalysts, as it is dominated by the oxygen and aluminum signals from the support. In addition to the signals due to O, Al and Pd, there is also a small amount of sodium on the surface of this catalyst. This is a residue of the NaOH, which was used to precipitate the palladium onto the support. As the O 1s peak at 531.0 eV from the Al_2O_3 support dominates the XPS spectra, only the binding energy region from 400 to 0 eV is used to facilitate the

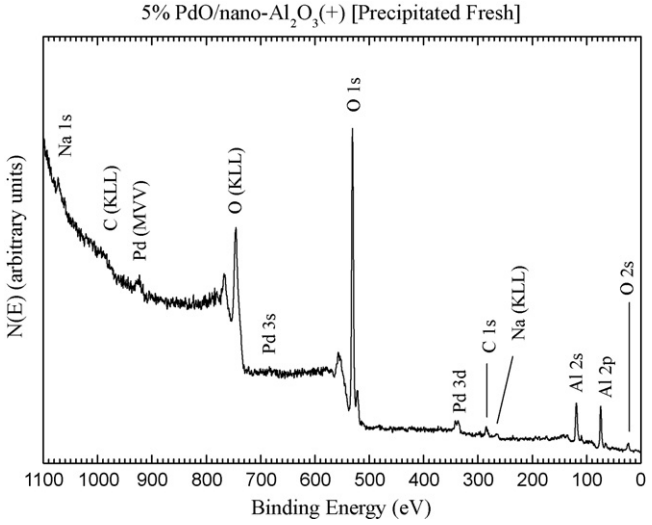

Fig. 2. XPS survey spectrum obtained from precipitated PdO/n-Al_2O_3(+).

comparison between the alumina-supported catalysts (Fig. 3). The compositional analysis for these catalysts is presented in Table 3. Considering the high dispersion of the precipitated PdO/n-Al_2O_3(+) it is surprising that the palladium signals are so weak on this catalyst. The XPS survey obtained from the commercial Pd/Al_2O_3 catalyst exhibits a more intense palladium peak, as is expected from

Table 3
Results from the XPS compositional analysis.

5% Pd catalysts[a]	Relative surface concentrations [%]				Peak area ratios					
	C 1s	0 1s	Pd 3d	A1 2p	Pd/Al	Pd/C	Al/C	Pd/O	Al/O	C/O
PdO/n-Al_2O_3(+) Pr. Fr.	8.5	50.9	1.3	39.4	0.03	0.15	4.65	0.02	0.77	0.17
PdO/n-Al_2O_3(+) Pr. Sp.	15.3	52.2	1.0	31.6	0.03	0.07	2.07	0.02	0.60	0.29
PdO/n-Al_2O_3(+) Pr. Sp, Ar^+	10.8	54.0	0.9	34.3	0.03	0.08	3.19	0.02	0.64	0.20
PdO/n-Al_2O_3(+) Im. Fr.	11.8	51.2	0.9	36.1	0.02	0.07	3.05	0.02	0.70	0.23
PdO/n-Al_2O_3(−) Pr. Fr.	12.6	48.8	5.0	33.6	0.15	0.40	2.72	0.10	0.69	0.26
PdO/y-Al_2O_3 Pr. Fr.	11.2	49.6	1.5	37.7	0.04	0.13	3.39	0.03	0.76	0.22
Pd/Al_2O_3 Com. Fr.	8.9	49.8	3.0	38.4	0.08	0.33	4.33	0.06	0.77	0.18
n-Al_2O_3(+) As received	13.2	52.2	0.0	34.6	0.00	0.00	2.63	0.00	0.66	0.25

[a] Pr.: precipitated; Fr.: fresh; Sp.: spent; Ar^+: Ar^+ sputtered; Im.: impregnated; Com.: commercial.

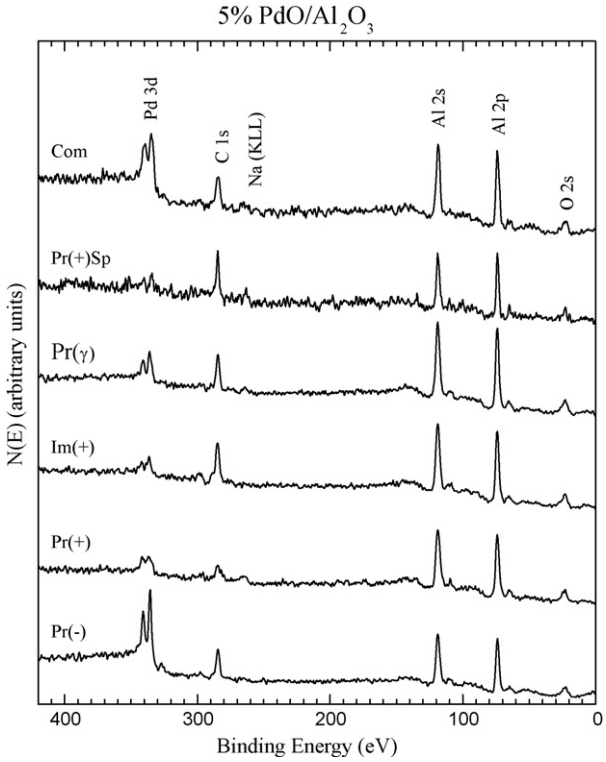

Fig. 3. XPS survey spectra obtained from Pr(−): precipitated PdO/n-Al_2O_3(−); Pr(+): precipitated PdO/n-Al_2O_3(+); Im(+): impregnated PdO/n-Al_2O_3(+); Pr(γ): precipitated PdO/γ-Al_2O_3; Pr(+)Sp: precipitated, spent PdO/n-Al_2O_3(+); and Com: commercial Pd/γ-Al_2O_3 catalysts.

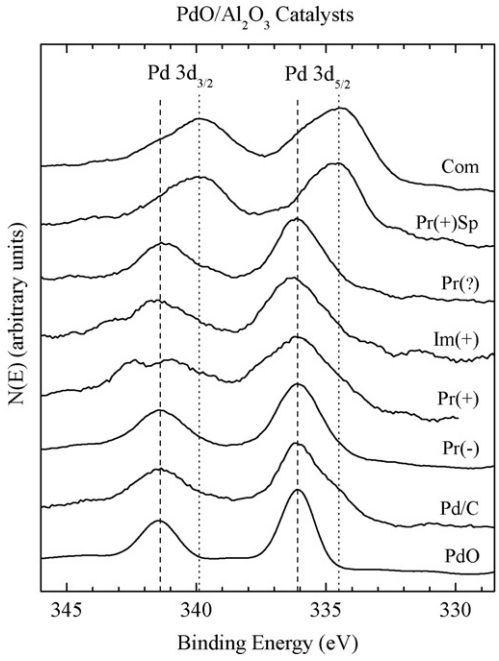

Fig. 4. Pd 3d XPS spectra obtained from PdO (PdO reference sample) and the following catalysts: Pd/C: commercial Pd/C; Pr(−): precipitated, PdO/n-Al_2O_3(−); Pr(+): precipitated PdO/n-Al_2O_3(+); Im(+): impregnated PdO/n-Al_2O_3(+); Pr(γ): precipitated PdO/γ-Al_2O_3; Pr(+)Sp: precipitated, spent PdO/n-Al_2O_3(+); and Com: commercial Pd/γ-Al_2O_3. The dashed lines mark the binding energies of Pd $3d_{5/2}$ and Pd $3d_{3/2}$ from PdO and the dotted lines denote the Pd $3d_{5/2}$ and Pd $3d_{3/2}$ from Pd metal.

the high palladium dispersion on this catalyst. However, the XPS signal is also dependent on the porosity of the support. For example, the large reduction in overall surface area after catalyst preparation for the n-Al_2O_3(+) support (see Tables 1 and 2) may, in addition to sintering, indicate that the palladium fills the voids in the support. Consequently, a large fraction of the added palladium is not present in the surface region probed with XPS (which is roughly 10 atomic layers from the surface [38]). The same phenomenon is observed to some extent on the impregnated PdO/n-Al_2O_3(+) catalyst.

In contrast, the palladium signal obtained from the low dispersion, precipitated PdO/n-Al_2O_3(−) catalyst is unexpectedly high. This is likely due to less efficient palladium penetration into the voids of this support, resulting in more palladium deposited in the near surface region probed with XPS (see also Section 3.4). The same appears to be true for the palladium precipitated onto the γ-Al_2O_3 support. For both supports [n-Al_2O_3(−) and γ-Al_2O_3], the palladium dispersions are very low and the reduction in the initial surface area of the support, compared to the overall surface area of the resulting catalyst, is considerably less than the reduction in surface area from the preparation of the n-Al_2O_3(+)-supported catalysts.

After reaction, the palladium signal from the precipitated PdO/n-Al_2O_3(+) catalyst is lower than before reaction, while the carbon signal is considerably higher. This has been observed before on Pd/C catalysts and was attributed to carbon-containing species on the surface covering the palladium as well as some palladium leaching from the surface [26]. As the palladium-to-alumina signals are similar on the fresh and spent catalysts (Table 3) the lower Pd signal on the spent catalyst appears to be mainly carbon deposition on the catalyst surface (which also covers the alumina support and lowers the Al peak intensities). This suggests that the amount of palladium leaching from the PdO/n-Al_2O_3(+) catalyst is low, which is important for possible catalyst regeneration.

3.3.2. High resolution spectra

The Pd 3d XPS spectra obtained from the palladium catalysts supported on the various alumina supports are presented in Fig. 4. The commercial Pd/C and Pd/Al_2O_3 catalysts, as well as a PdO sample, have been included for comparison. The major species on most catalysts, including Pd/C, is located at a binding energy of 336.1 eV, which is consistent with the reference value reported for the Pd $3d_{5/2}$ peak of PdO (336.3 eV [39,40] with values reported between 335.6 and 337.1 eV [41]). In contrast, the major species on the commercial Pd/Al_2O_3 catalyst is located at 334.5 eV, which is lower than that reported for bulk Pd metal (334.9 eV [39]), but is in agreement with values typically observed for surface Pd^0 in high dispersion catalysts [42]. A small shoulder at 336.1 eV indicates that there is some surface PdO on this catalyst. There is also an indication of a Pd species with an oxidation state higher than PdO on both the commercial Pd/C and Pd/Al_2O_3 catalysts (Fig. 5A). This could be a $Pd(OH)_2$ or a PdO_x species ($x > 1$). These results, and the lower yield from a reduced catalyst, are consistent with PdO being the active phase on these catalysts and explain why the commercial Pd/Al_2O_3 catalyst exhibits little if any activity in these reactions, while the Pd/C (or more accurately PdO/C) is an active catalyst.

The Pd $3d_{5/2}$ peak obtained from the spent PdO/n-Al_2O_3(+) catalyst is located at a low binding energy (334.9 eV), which is indicative of Pd metal as has been observed previously for spent Pd/C catalysts [26]. Peak fitting reveal that the amount of PdO is less on this catalyst compared with the commercial Pd/Al_2O_3 catalyst (Fig. 5A). While the contribution from the PdO_x or $Pd(OH)_2$ appears to be higher on the spent PdO/n-Al_2O_3(+) catalyst according to the peak fitting results, this peak is likely overestimated in the peak fitting due to the higher signal-to-noise in the spectra obtained from the spent PdO/n-Al_2O_3(+) catalyst compared with those from the commercial Pd/Al_2O_3 catalyst. The low concentration of PdO or PdO_x on the surface of the spent catalyst is a potential reason for catalyst deactivation in these systems, as these catalysts are likely limited

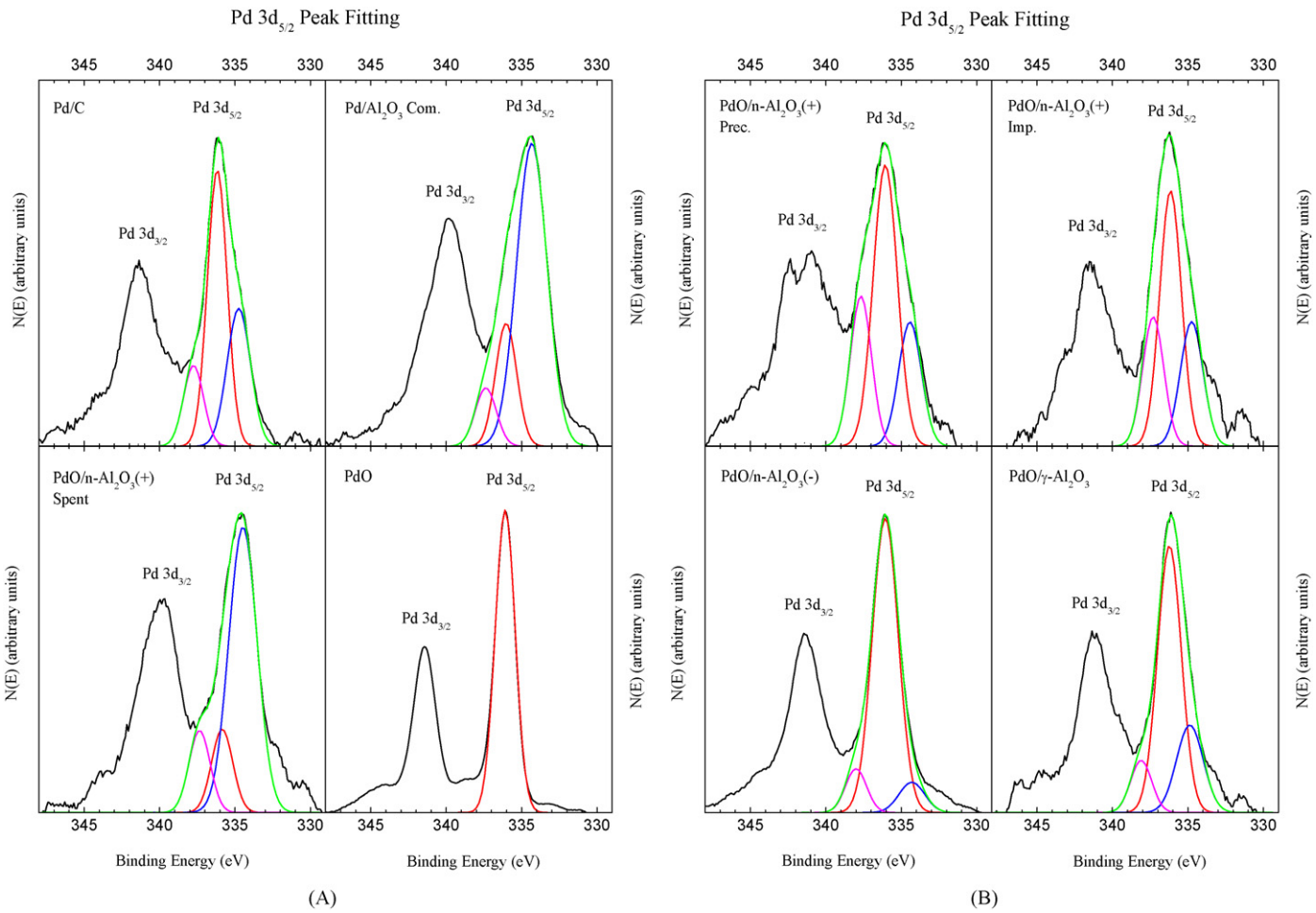

Fig. 5. Peak fitting results for the Pd $3d_{5/2}$ peaks obtained from the catalysts under investigation. ( ) Actual data, ( ) Pd metal peak at ~334.6 eV, ( ) PdO peak at ~336.1 eV, ( ) PdO_x ($x > 1$) or $Pd(OH)_2$ peak at ~337.6 eV, and ( ) sum of model peaks. (For interpretation of the references to color in this figure legend, the reader is referred to the web version of the article.)

by the reoxidation of the palladium species to close the catalytic cycle (see Fig. 1).

While the major species is PdO on all the prepared fresh catalysts, the Pd 3d peak widths vary significantly on the different alumina supports. The Pd 3d peaks obtained from the fresh catalysts (impregnated and precipitated) supported on the nanoparticle Al_2O_3(+) are considerably broader than those obtained from the n-Al_2O_3(−)- and γ-Al_2O_3-supported catalysts (Fig. 4). The distinct shoulders at 337.3–337.6 and 334.4–334.8 eV on the PdO/n-Al_2O_3(+) catalysts are due to larger contributions from the PdO_x (or $Pd(OH)_2$) and Pd^0 states respectively compared to the other catalysts (Fig. 5B and Table 4). As the PdO/n-Al_2O_3(+) catalysts are the most active of the alumina-supported catalysts, it is possible that the presence of PdO_x ($x > 1$) is necessary to ensure a high catalytic activity. According to the reaction mechanism presented in Fig. 1, a more electrophilic palladium (such as a state at BEs of 337.3–338.1 eV) is likely more reactive in the first coordination of the reactant and may facilitate H^+ abstraction compared to PdO. It is also possible that a Pd^0 and PdO_x pair (Pd^0–Pd^{y+}, where $x \geq 1$ and $y \geq 2$) is responsible for the high catalytic activity observed for these catalysts. Yet, another possibility is that the "PdO_x" ($x > 1$) phase observed reveals palladium–support

Table 4
Results from the XPS peak fitting of the Pd $3d_{5/2}$ peaks of the catalyst in the study.

	Catalyst Description	Pd/C Fresh	PdO/n-Al_2O_3(−) Prec. Fresh	PdO/n-Al_2O_3(+) Prec. Fresh	PdO/n-Al_2O_3(+) Imp. Fresh	PdO/y-Al_2O_3 BM Fresh	PdO/n-Al_2O_3(+) Prec. Spent	Pd/Al_2O_3 Com. Fresh
PdO	Peak position	336.1	336.1	336.1	336.1	336.2	335.9	336
	Peak width	1.5	2.0	1.9	1.7	1.8	1.7	1.7
	Peak area	670	2600	578	315	722	300	495
	Peak area %	53	82	53	50	65	15	20
Pd	Peak position	334.7	334.4	334.4	334.8	334.8	334.5	334.3
	Peak width	1.8	2.0	1.7	1.7	2.1	2.2	2.3
	Peak area	395	265	241	160	265	1375	1760
	Peak area %	31	8	22	25	24	70	71
PdO_x ($x > 1$)	Peak position	337.7	338	337.6	337.3	338.1	337.3	337.3
	Peak width	1.6	1.7	1.7	1.7	1.7	1.6	1.6
	Peak area	198	315	270	155	125	295	235
	Peak area %	15	10	25	25	11	15	9

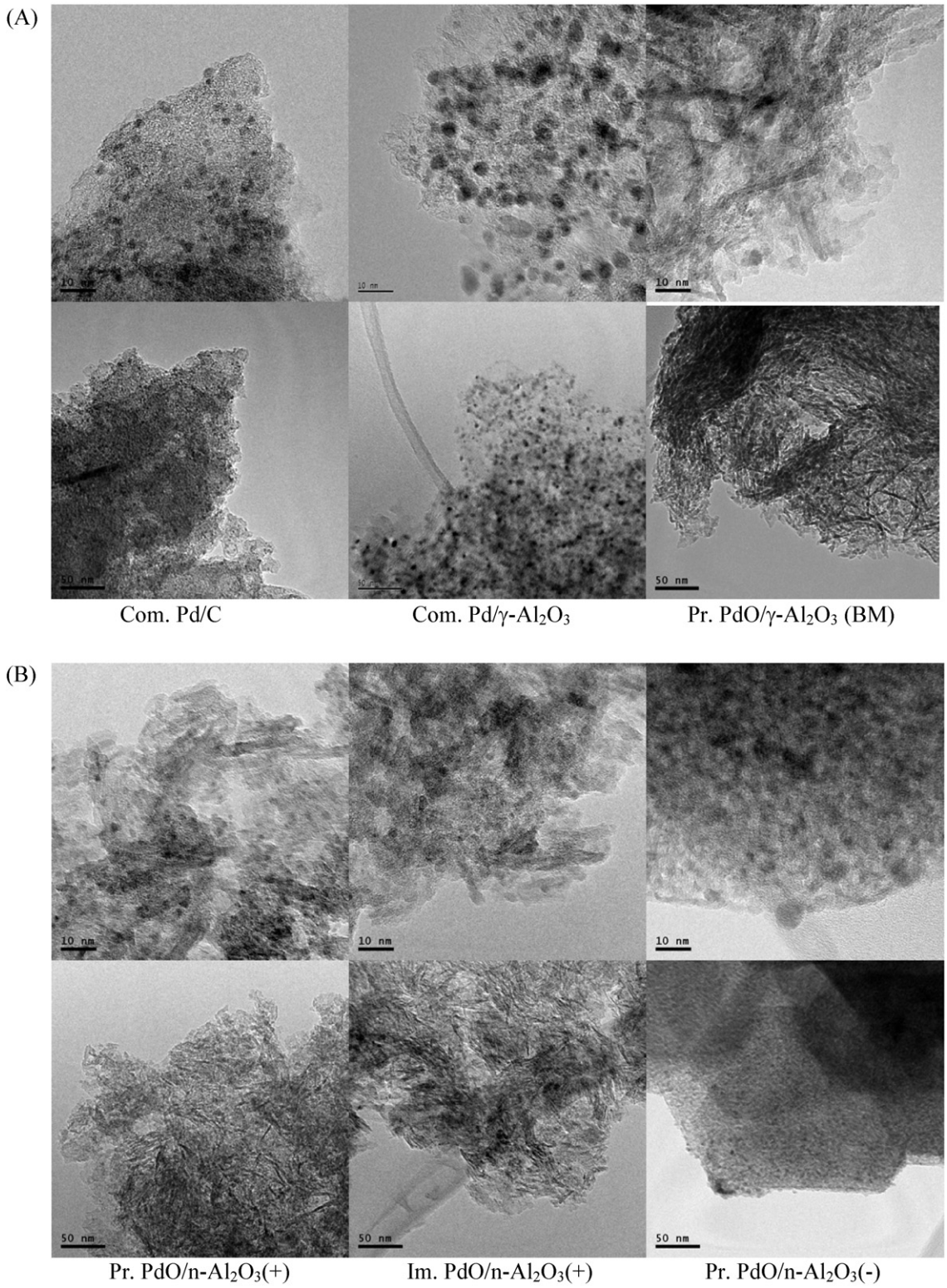

Fig. 6. TEM pictures obtained from the catalysts under investigation at two different magnifications (top: scale bar = 10 nm, bottom: scale bar = 50 nm). (A) Left: commercial Pd/C; middle: commercial Pd/γ-Al_2O_3; right: precipitated PdO/γ-Al_2O_3 (bimodal). (B) Left: precipitated PdO/n-Al_2O_3(+); middle: impregnated PdO/n-Al_2O_3(+); right: precipitated PdO/n-Al_2O_3(−).

interactions which result in a palladium phase that is easier to reoxidize.

The similarities in the Pd 3d peak shapes of the impregnated and the precipitated fresh catalysts are in agreement with the higher activities observed from the impregnated catalyst in the present study compared to the previous results. It is difficult to explain why some preparations of the impregnated catalyst would be inferior to the precipitated catalyst on the basis of XPS.

Due to the low dispersions of the PdO/n-Al_2O_3(−) and PdO/γ-Al_2O_3 catalysts, most of the palladium signal from these catalysts arise from non-active species, i.e. species that are below the outermost surface palladium. Consequently, discerning the active

surface species for these catalysts would be challenging at best. It is therefore not surprising that the Pd 3d peaks obtained from these catalysts are similar (Fig. 4), even though their activities are significantly different. The peak fitting reveal that the contributions from both the PdO_x and the Pd^0 states are higher on the PdO/γ-Al_2O_3 versus the PdO/n-Al_2O_3(−) catalyst (Fig. 5B). This is in agreement with the more active catalyst being the one with the broader Pd $3d_{5/2}$ peak, i.e. the PdO/γ-Al_2O_3 catalyst.

The O 1s binding energy region is dominated by the Al_2O_3 oxygen at 531.0 eV on these catalysts, so no significant differences in the O 1s peaks between the catalysts can be observed (not shown). The Al 2p peaks at 74 eV obtained from these catalysts are also not informative (not shown).

3.4. TEM/EDS data

The prepared alumina-supported catalysts (after calcination) and the commercial Pd/C and Pd/Al_2O_3 (as received) were subjected to TEM analysis.

3.4.1. Commercial catalysts and supports

The TEM obtained from the commercial catalysts are typical, showing fine, nanometer-sized support features and relatively uniform distribution of Pd particles on the surface of the support (visible as darker spots in the TEM pictures, Fig. 6A, left and middle). The smaller Pd/PdO particle size on the Pd/C compared with the Pd/Al_2O_3 catalyst is in agreement with the calculated particle size from the palladium surface areas of the two catalysts (Table 2). The PdO precipitated onto the bimodal γ-alumina (γ-Al_2O_3) looks very different from the commercial catalysts. It is difficult to discern the PdO particles on this catalyst and it appears that the palladium oxide particles and their particle sizes are inhomogeneously distributed on the surface of this support. EDS scans on this catalyst (not shown) reveal that there are some large palladium oxide particles on this catalyst and their particle size is indeed consistent with the >50 nm reported from the Pd surface area measurements on a reduced catalyst. At a lower magnification (Fig. 6A bottom right), it is evident that the structure of the support is very different from the carbon and alumina supports of the commercial catalysts. The support appears to consist of interlaced nanometer-sized rods or strands, and this is similar to the n-Al_2O_3(+) support (Fig. 6B bottom left).

3.4.2. Catalyst supported on nanoparticle alumina

The PdO precipitated onto the n-Al_2O_3(+) support appears to result in a relatively uniform distribution of palladium oxide particles on the surface (Fig. 6B, left). The 2-nm Pd particle size calculated from metal surface area measurements after catalyst reduction are reasonably consistent with the PdO particle size observed in the TEM picture of the unreduced catalyst. The palladium oxide distribution on the impregnated PdO/n-Al_2O_3(+) catalyst is not as uniform compared to the precipitated catalyst (Fig. 6B, middle). Some particles, although not all, are larger on the impregnated compared with the precipitated catalyst, which is consistent with the lower dispersions and the average particle size calculated from the palladium surface area measurements. The structure of the n-Al_2O_3(+) support exhibit some similarity with the BM γ-Al_2O_3 support in that it does contain some nanometer-sized strands. However, the n-Al_2O_3(+) also contains finer structures in the form of small irregular particles, which are on the order of a few nanometers.

The structure of the n-Al_2O_3(−) support is very different from the n-Al_2O_3(+) and γ-Al_2O_3 supports. It appears to consist of close-packed larger crystals (Fig. 6B, right) compared with the small irregular particles and strands of the n-Al_2O_3(+) and γ-Al_2O_3 supports. From the lower magnification it appears that the palladium oxide is deposited as fairly large crystals on the outermost surface of this support. The PdO particle sizes appear to be smaller than on the PdO/γ-Al_2O_3 support, which again is consistent with the Pd particle sizes obtained from the Pd surface area measurements. More palladium oxide on the outermost surface of this support also explains the higher Pd peak intensities in the XPS data obtained from this catalyst compared to the catalysts supported on n-Al_2O_3(+).

The PdO particle sizes observed in the TEM micrographs are consistent with the Pd particle sizes measured from the catalysts after reduction, which suggests that the reduction treatment does not significantly alter the distribution of palladium on the surfaces of these supports. The fact that the PdO/γ-Al_2O_3 is moderately active despite the low palladium surface area is consistent with our hypothesis that supports with low-coordination corner and edge sites can lead to highly active catalysts, as this support does have significant fine structure on the nanometer scale. It is our belief that a high number of low-coordination sites, such as corners and edges [43], can result in strong metal support interactions and unique catalytic properties. Although the support structure in the case of the PdO/γ-Al_2O_3 catalyst does not lead to a high palladium surface area, it appears that some palladium on this surface is highly active, perhaps due to favorable palladium–support interactions at the low-coordination sites. Compared with the n-Al_2O_3(+) there are fewer of these low-coordination sites on the γ-Al_2O_3 support. This hypothesis would also explain why the PdO/n-Al_2O_3(−) is not a very active catalyst, since this support does not appear to have the same structure with low-coordination sites.

3.5. XRD data analysis

The supports and prepared catalysts were subjected to XRD analysis to determine any crystal structure present and obtain a measure of the crystalline particle sizes.

3.5.1. Alumina supports

The XRD patterns obtained from the different alumina supports used in this study are presented in Fig. 7A. All supports except the n-Al_2O_3(+) are composed of γ-Al_2O_3 [44]. The pattern obtained from the n-Al_2O_3(+) is unexpected as the supplier indicated the alumina to be amorphous [31]. When compared to reference patterns from the JCPDS data base, the phase present in the n-Al_2O_3(+) support was identified as bohemite (aluminum oxide hydroxide, AlO(OH)) [45]. When the n-Al_2O_3(+) support is calcined at higher temperatures (above 350 °C), the AlO(OH) releases water and is converted to the γ-Al_2O_3 phase (Eq. (2) and Fig. 7A). The n-Al_2O_3(+) sample was therefore analyzed using thermogravimetric analysis (TGA) to determine how much weight is lost in this process. After drying at 105 °C to remove any absorbed moisture, the additional weight lost from the n-Al_2O_3(+) sample would correspond to ~85% AlO(OH) by weight. While this support thus more accurately should be referred to as nanoparticle AlO(OH), the n-Al_2O_3(+) label is kept for reasons of consistency.

$$2AlO(OH) \xrightarrow{\Delta} Al_2O_3 + H_2O \quad (2)$$

It is possible that the hydroxyl groups on the aluminum oxide hydroxide "n-Al_2O_3(+)" support results in favorable interactions with the palladium ions in the deposition step giving very high dispersions compared to the n-Al_2O_3(−) and BM-Al_2O_3 supports, which are composed of γ-Al_2O_3. In the case of the PdO/BM-Al_2O_3 catalyst, the nanometer-sized features of the support may explain why this catalyst is more active than the PdO/n-Al_2O_3(−) despite the low palladium dispersion. Both the n-Al_2O_3(+) and the BM-Al_2O_3 supports exhibit nanometer-sized support features, which could lead to favorable palladium–support interactions, that are absent on the n-Al_2O_3(−) support.

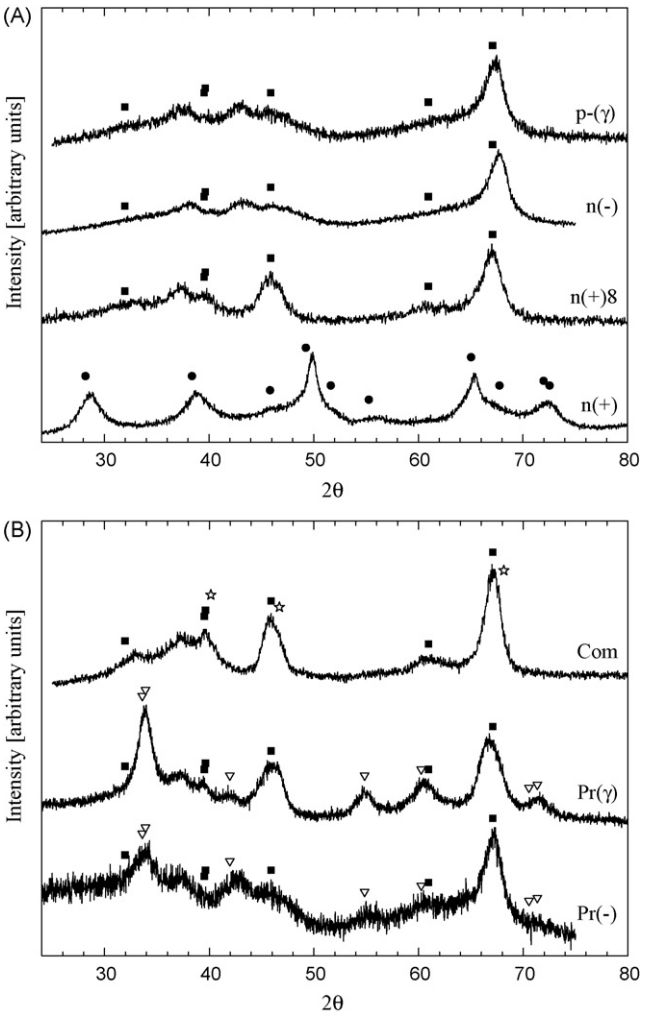

Fig. 7. XRD patterns obtained from selected supports and catalysts. (A) n(+): n-Al_2O_3(+) as received (batch 2); n(+)8: n-Al_2O_3(+) calcined at 800 °C; n(−): n-Al_2O_3(−) as received; and p-(γ): porous, bimodal γ-Al_2O_3, as received. (B) Pd(−): precipitated PdO/n-Al_2O_3(−); Pr(γ): precipitated PdO/γ-Al_2O_3; and Com: commercial Pd/γ-Al_2O_3. The legend for the data is as follows: (■) γ-Al_2O_3, (●) AlO(OH) (bohemite), (☆) Pd metal, and (▽) PdO (tetragonal).

3.5.2. Fresh catalysts

The XRD patterns obtained from the catalysts under investigation are presented in Figs.7B–9. The PdO [46] peak intensities for the fresh 5% PdO/n-Al_2O_3(−) are surprisingly low considering its low Pd surface area and, thus, large PdO particle sizes (Fig. 7B). This indicates that the PdO on this catalyst is mainly amorphous, i.e. most of the PdO is XRD invisible as it has no long-range order. Due to the amorphous nature of this catalyst, determining the PdO particle size on this catalyst is subject to significant errors. Therefore, the PdO particle size determined from the XRD data is not included in Table 5. In contrast, the PdO peak intensities in the XRD pattern obtained from the PdO/γ-Al_2O_3 catalyst are significant, in agreement with the low palladium surface area observed on this catalyst. However, the PdO particle sizes calculated for this catalyst from the Scherrer equation and the full-width-at-half-maximum (FWHM), gives an average particle size of crystalline PdO in the range of ~5 nm (Table 5). This is significantly smaller than the particle size determined from the measured Pd surface area on the reduced catalyst. Consequently, a significant amount of the PdO on the surface of this catalyst is also amorphous. This is supported by the fact that considerable sintering, i.e. from 5 to >50 nm, of the palladium during the low temperature reduction of the Pd surface

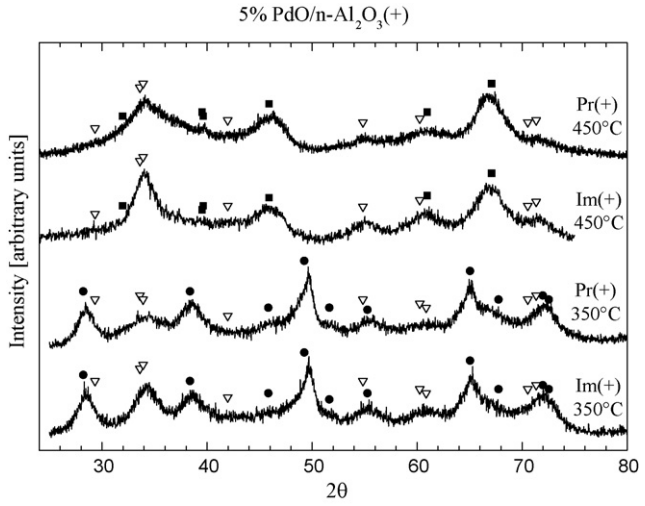

Fig. 8. XRD patterns obtained from impregnated and precipitated PdO/n-Al_2O_3(+) calcined at 350 and 450 °C. Im(+): impregnated PdO/n-Al_2O_3(+); and Pr(+): precipitated PdO/n-Al_2O_3(+). The legend for the data is as follows: (●) AlO(OH) (bohemite), (▽) PdO (tetragonal), and (■) γ-Al_2O_3.

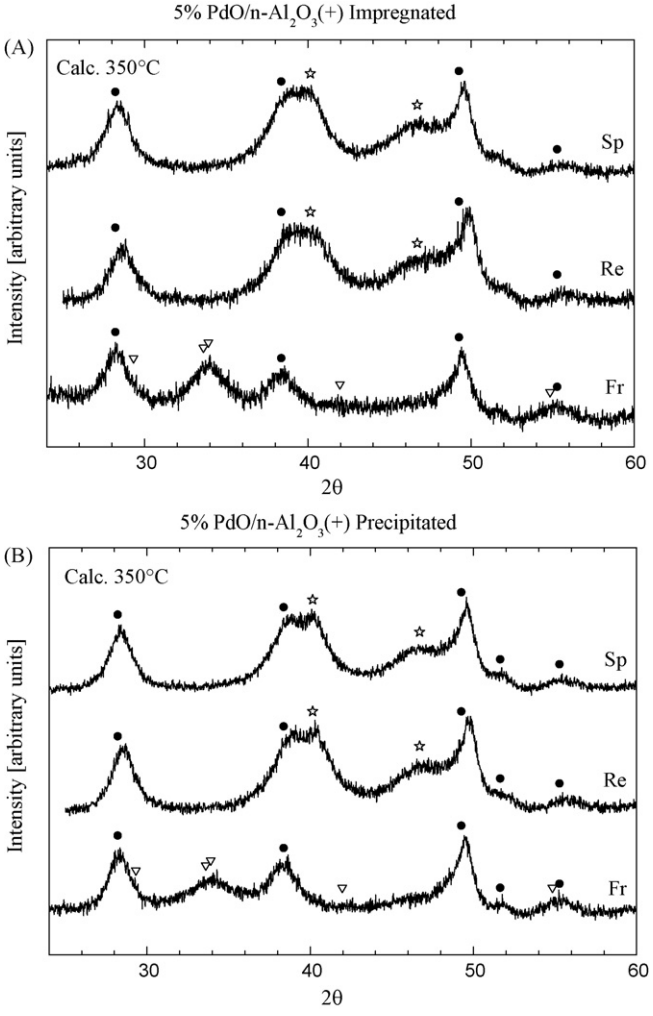

Fig. 9. XRD patterns obtained from impregnated and precipitated PdO/n-Al_2O_3(+). (A) Impregnated catalysts, Fr: fresh; Re: reduced; and Sp: spent. (B) Precipitated catalysts, Fr: fresh; Re: reduced; and Sp: spent. The legend for the data is as follows: (●) AlO(OH) (bohemite), (☆) Pd metal, and (▽) PdO (tetragonal).

Table 5
Pd and PdO particle sizes determined from the XRD data using the Scherrer equation and the full-width-at-half-maximum (FWHM).

Catalyst	PdO particle size [nm]	Pd particle size [nm]
PdO/n-Al_2O_3(+) Prec. Fresh	2.9	–
PdO/n-Al_2O_3(+) Prec. Reduced	–	3.4
PdO/n-Al_2O_3(+) Prec. Spent	–	3.5
PdO/n-Al_2O_3(+) Imp. Fresh	3.7	–
PdO/n-Al_2O_3(+) Imp. Reduced	–	2.9
PdO/n-Al_2O_3(+) Imp. Spent	–	3.3
PdO/y-Al_2O_3 Prec. Fresh	5.1	–

area measurements is unlikely and the TEM measurements also indicate large PdO particles. This said, the PdO on the PdO/γ-Al_2O_3 catalyst is much more crystalline than the PdO on the n-Al_2O_3(−) support. The more crystalline PdO on the PdO/γ-Al_2O_3 catalyst may be taken as a indication of a more favorable metal–support interaction compared with the PdO/n-Al_2O_3(−), which could lead to a higher catalytic activity.

As expected, no PdO can be detected on the commercial Pd/Al_2O_3 catalyst and Pd metal is difficult to discern since the Pd^0 peaks [47] overlap with those of the γ-Al_2O_3 support (Fig. 7B). The only Pd metal peak that can be distinguished from the support peaks is the Pd(1 1 1) at $2\theta = 40.1°$. Apart from this small peak, the pattern from the Pd/Al_2O_3 catalyst is very similar to the one obtained from the n-Al_2O_3(+) support calcined at 800 °C (Fig. 7A).

Despite the high dispersions and the low palladium loadings, the presence of PdO is evident in the XRD pattern obtained from the fresh 5% PdO/n-Al_2O_3(+) catalysts (Figs. 8 and 9). The XRD patterns in Fig. 8 reveal the differences in support structure between calcinations at 350 and 450 °C. Evidently, the phase transformation from AlO(OH) to γ-Al_2O_3 occurs somewhere in this temperature range, as catalysts calcined at 350 °C contain only the AlO(OH) phase while catalysts calcined at 450 °C contain only the γ-Al_2O_3 phase (Fig. 8). This phase transformation does not appear to affect the palladium on the surface significantly as the catalytic activities from the 350 °C- and 450 °C-calcined catalysts are similar. For example, the PdO/n-Al_2O_3(+) catalyst results in ∼52 g of product/g Pd if calcined at 350 °C and ∼50 g product/g Pd when calcined at 450 °C. This is within the standard deviations of ±6–10% of the experiments. The low palladium oxide signal and overlapping features with γ-Al_2O_3 or bohemite makes it difficult to determine the peak widths of the palladium oxide peaks. Consequently, calculating the particle sizes using the Scherrer equation is challenging at best for these catalysts. Furthermore, as long-range order in the crystalline structure is necessary to give an XRD signal, any PdO particles below 1–2 nm will be XRD invisible. For this reason, XRD is expected to overestimate the average particle sizes of high dispersion catalysts, unless of course the particles are amorphous, as is the case for the PdO/γ-Al_2O_3 and PdO/n-Al_2O_3(−) catalysts. Despite the limitations of the XRD technique, it is evident that the particle sizes calculated from the XRD peak widths are consistent with the particle size trend obtained from the measured palladium surface areas of the fresh impregnated and precipitated catalysts (see Tables 2 and 5). At both calcination temperatures (350 and 450 °C), the precipitated catalysts have the broader peaks, as expected from the higher palladium surface areas and smaller particle sizes measured on these catalysts, compared to the impregnated ones. Using a software to deconvolute the peaks of the catalysts calcined at 350 °C, the PdO particle sizes on the impregnated and precipitated catalysts are 3.7 and 2.9 nm, respectively (Table 5). The trend in particle size is in very good agreement with the data obtained from the Pd surface area measurements (3.3 and 2.1 nm), considering that the XRD particle sizes are expected to be overestimated due to the limitations of XRD in this size range.

3.5.3. Reduced catalysts

The XRD patterns obtained from the reduced precipitated and impregnated catalysts reveal that the PdO is completely reduced to Pd metal during the mild reduction conditions (Fig. 9A and B). No peaks due to PdO can be detected on the reduced catalysts and new peaks due to Pd metal are evident. Based on the peak widths, the Pd particle sizes on these catalysts are 2.9 (impregnated Pd/n-Al_2O_3(+)) and 3.4 nm (precipitated Pd/n-Al_2O_3(+)). While the PdO particle sizes were smaller on the fresh precipitated Pd/n-Al_2O_3(+) catalyst (2.9 nm) compared to the Pd particle sizes after reduction, the differences are not significant considering the uncertainties in determining the particle sizes using a peak deconvolution routine and the limitations of XRD particle sizing in this size range. Therefore, reduction treatment before the Pd surface area measurements does not cause significant sintering.

3.5.4. Spent catalysts

The XRD patterns obtained from the spent catalysts are very similar to the XRD patterns obtained from the reduced catalysts (Fig. 9A and B). The fact that no PdO-related peaks are visible indicates that the PdO particles are fully reduced during the reaction, as opposed to just the surface and near surface PdO. The FWHM of the spent impregnated and precipitated catalysts give particles sizes on the order of 3.3–3.5 nm, which is similar to the Pd particle sizes on the reduced catalysts. The similarity in Pd metal peak widths and signal intensity between the reduced and spent catalysts indicates that there is no significant sintering of the palladium on the surface during reaction. Furthermore, the XRD data does not reveal any evidence of significant leaching of the palladium from these catalysts. Consequently, the XRD data supports our conclusion from the XPS section, namely that the catalysts after reaction are covered with carbon and have not lost a significant amount of palladium due to leaching. This carbon is not removed during the reductive treatment, and results in low amounts of CO adsorbed on the spent catalysts during the CO chemisorption measurements (Table 2).

As the PdO on the surface is fully reduced during the reaction, these reactions are likely limited by reoxidation of the formed palladium as the oxygen is only present in the gas phase above the reaction medium.

4. Conclusions

This study supports the previous conclusion that PdO is necessary for an active catalyst. After reaction both XPS and XRD reveal that the PdO is completely (both the surface and the crystalline bulk) reduced to Pd metal. Oxygen supply to the catalyst may thus be the main limitation in this reaction. The XPS data also indicates that the catalyst surface after reaction is covered with carbon, which could indicate poisoning or coking. As the Pd/Al ratio is not significantly reduced after reaction, leaching does not appear to be a significant deactivation pathway for the PdO/n-Al_2O_3(+) catalyst.

The most active catalysts, the impregnated and precipitated PdO/n-Al_2O_3(+) catalysts, have very broad Pd 3d peaks, indicating the presence of both PdO_2 and Pd^0 in addition to the PdO. The presence of PdO_x ($x > 1$) or a Pd^0–Pd^{y+} ($y \geq 1$) pair, may be beneficial to the reaction and could reveal palladium–support interactions that result in a palladium phase that is easier to reoxidize.

The structure and morphology of the support is also important in the preparation of active palladium catalysts. The n-Al_2O_3(+) support can yield very high dispersions and high catalytic activities,

revealing favorable palladium–support interactions. This support exhibits nm-sized fine structure and corroborates our hypothesis that low-coordination sites on a support can result in strong metal–support interactions and very active catalysts.

It is possible that PdO crystals below a certain particle size are the most active in this reaction, which would explain why the catalytic activity does not exhibit a simple correlation with the measured palladium surface area.

Acknowledgments

Acknowledgment is made to the Donors of the American Chemical Society Petroleum Research Fund for support of this research. XRD measurements were performed at the Major Analytical Instrumentation Center (MAIC) at the University of Florida. The authors are thankful for the advice and instruction of Dr. Valentin Craciun. The authors also wish to thank Dr. Kerry Siebein at MAIC, who recorded the TEM images. Dr. Amelia Dempere, the director of MAIC, is gratefully acknowledged for valuable advice and fruitful discussion of the TEM data. The BET and TGA data were collected at the Particle Engineering Research Center at the University of Florida. The authors are grateful for the training on the BET machine provided by Mr. Gill Brubaker and on the TGA instrument by Mr. Nate Stevens. In addition, the authors wish to thank Justin Dodson for running the n-Al_2O_3(+) TGA sample for us.

References

[1] P.M. Maitlis, The Organic Chemistry of Palladium, Academic Press, New York, 1971.
[2] J. Tsuji, Palladium Reagents and Catalysis: Innovation in Organic Synthesis, Wiley, Chichester, UK, 1995.
[3] J.-L. Malleron, J.-C. Fiaud, J.-Y. Legros, Handbook of Palladium—Catalyzed Organic Reactions, Academic Press Limited, London, UK, 1997.
[4] P. Gélin, M. Primet, Appl. Catal. B 39 (2002) 1.
[5] T.W.G. Solomons, Organic Chemistry, John Wiley & Sons, Inc., New York, 1996, pp. 291–293.
[6] D. Ciuparu, A. Ensuque, F. Bozon-Verduraz, Appl. Catal. A 326 (2007) 130.
[7] M. Besson, P. Gallezot, Catal. Today 57 (2000) 127.
[8] A.K. Santra, D.W. Goodman, Electrochim. Acta 47 (2002) 3595.
[9] S.-H. Oh, G.B. Hoflund, J. Catal. 245 (2007) 35.
[10] T.V. Choudhary, S. Banerjee, V.R. Choudhary, Appl. Catal. A 234 (2002) 1.
[11] D. Ciuparu, M.R. Lyubovsky, E. Altman, L.D. Pfefferle, A. Datye, Catal. Rev. Sci. Eng. 44 (2002) 593.
[12] M. Hosseini, S. Siffert, H.L. Tidahy, R. Cousin, J.-F. Lamonier, A. Aboukais, A. Vantomme, M. Roussel, B.-L. Su, Catal. Today 122 (2007) 391.
[13] P. Papaefthimiou, T. Ioannides, X.E. Verykios, Appl. Catal. B 13 (1997) 175.
[14] E.M. Cordi, J.L. Falconer, J. Catal. 162 (1996) 104.
[15] C. Kaes, A. Katz, M.W. Hosseini, Chem. Rev. 100 (2000) 3553.
[16] V. Balzani, A. Juris, M. Venturi, S. Campagna, S. Serroni, Chem. Rev. 96 (1996) 759.
[17] K. Kalyanasundaram, Coord. Chem. Rev. 46 (1982) 159.
[18] R.C. Evans, P. Douglas, C.J. Winscom, Coord. Chem. Rev. 250 (2006) 2093.
[19] L. Gámiz-Gracia, A.M. Garcıía-Campaña, J.J. Soto-Chinchilla, J.F. Huertas-Pérez, A. González-Casado, Trends Anal. Chem. 24 (2005) 927.
[20] C.D. Clark, M.Z. Hoffman, Coord. Chem. Rev. 159 (1997) 359.
[21] N.M.L. Hansen, K. Jankova, S. Hvilsted, Eur. Polym. J. 43 (2007) 255.
[22] D.L. Feldheim, C.J. Baldy, P. Sebring, S.M. Hendrickson, C.M. Elliott, J. Electrochem. Soc. 142 (1995) 3366.
[23] W. Wu, S. Chen, F. Tsai, Tetrahedron Lett. 47 (2006) 9267.
[24] A. Launkonis, D. Lay, A. Mau, A. Saragesor, W. Sasse, Aust. J. Chem. 39 (1986) 1053.
[25] C.A. Páez, N.J. Castellanos, F.O. Martínez, F. Ziarelli, G. Agrifoglio, E.A. Páez-Mozo, H. Arzoumanian, Catal. Today 133–135 (2008) 619.
[26] H. Hagelin, B. Hedman, I. Orabona, T. Åkermark, B. Åkermark, C.A. Klug, J. Mol. Catal. A 164 (2000) 137.
[27] G.D.F. Jackson, W.H.F. Sasse, C.P. Whittle, Aust. J. Chem. 16 (1963) 1126.
[28] P.E. Rosevear, W.H.F. Sasse, J. Heterocycl. Chem. 8 (1971) 483.
[29] P.E. Rosevear, W.H. Sasse, Patent Appl. No. 40930/72 (1973), p. 1.
[30] S. Munavalli, M. Gratzel, Chem. Ind. (1987) 722.
[31] n-Al_2O_3(+): NanoScale NanoActive Alumina Plus, http://www.nanoscalecorp.com/content.php/chemicals/powders/. Properties: ≥550 m^2/g.
[32] Alfa Aesar TiO_2 catalyst support, Properties: Anatase with surface area 150 m^2/g.
[33] L.M. Neal, H. Hagelin-Weaver, J. Mol. Catal. A 284 (2008) 141.
[34] L.M. Neal, H. Hagelin-Weaver, J. Mol. Catal. A 307 (2009) 29.
[35] n-Al_2O_3(−): NanoActive Aluminum Oxide from NanoScale, http://www.nanoscalecorp.com/content.php/chemicals/powders/. Properties: ≥275 m^2/g.
[36] γ-Al_2O_3: A bimodal, high surface area, gamma-alumina catalyst support from Alfa Aesar. Properties: SA = 255 m^2/g.
[37] C.D. Wagner, W.M. Riggs, L.E. Davis, J.F. Moulder, G.E. Muilenberg (Eds.), Handbook of X-ray Photoelectron Spectroscopy, Perkin-Elmer Corp, Eden Prairie, MN, 1979.
[38] J.C. Rivière, S. Myhra (Eds.), Handbook of Surface and Interface Analysis, Marcel Dekker, New York, 1998, pp. 57–158.
[39] J.F. Moulder, W.F. Stickel, P.E. Sobol, K.D. Bomben, Handbook of X-ray Photoelectron Spectroscopy, Physical-Electronics Inc., Eden Prairie, MN, 1995.
[40] K.S. Kim, A.F. Gossmann, N. Winograd, Anal. Chem. 46 (1974) 197.
[41] National Institute of Standards and Technology, NIST on-Line XPS Database. http://srdata.nist.gov/xps/intro.aspx (accessed 28.10.08).
[42] C.E. Gigola, M.S. Moreno, I. Costilla, M.D. Sanchez, Appl. Surf. Sci. 254 (2007) 325.
[43] L. Guczi, A. Beck, A. Horváth, D. Horváth, Top. Catal. 19 (2002) 157.
[44] JCPDS International Center for Diffraction Data # 10-0425, 1996 [ref database] (gamma alumina).
[45] JCPDS International Center for Diffraction Data # 21-1307, 1996 [ref database] (Bohemite).
[46] JCPDS International Center for Diffraction Data # 06-0515, 1996 [ref database] (PdO).
[47] JCPDS International Center for Diffraction Data # 5-681, 1996 [ref database] (Pd metal).